DMD Fast Forward. Published on January 23, 2019 as DOI: 10.1124/dmd.118.084624
This article has not been copyedited and formatted. The final version may differ from this version.

Title Page

Hepatocyte Concentrations of Imaging Compounds Associated with Transporter Inhibition: Evidence in perfused rat livers

Pierre Bonnaventure, Fabien Cusin, and Catherine M Pastor

Department of Radiology, Hôpitaux Universitaires de Genève, Geneva, Switzerland PB, FC, CMP) and Laboratory of Imaging Biomarkers, Centre of Research on Inflammation, UMR 1149 INSERM and University Paris Diderot, France (CMP)

Running Page

Running title:

Drug hepatocyte concentrations and transporter inhibition

Address for correspondence:

Catherine M Pastor, MD, PhD
Department of Radiology
Hôpitaux Universitaires de Genève
Rue Gabrielle-Perret-Gentil, 4
1205 Geneva, Switzerland
Phone: ++41 22 372 45 68
catherine.pastor@unige.ch

Number of text pages: 26

Number of tables: 1

Figures: 5

References: 41

Number of words in abstract: 231

Number of words in introduction: 706

Number of words in discussion: 878

List of nonstandard abbreviations:

Gadobenate dimeglumine, MultiHance®, Bracco Imaging (BOPTA); Gadopentetate dimeglumine, Magnevist®, Bayer Pharma (DTPA); Technescan DTPA® b.e.imaging, Schwyz, Switzerland (DTPA); Mebrofenin, Choletec®, Bracco Imaging (MEB); magnetic resonance imaging (MRI); single photon emission computed tomography (SPECT); organic anion transporting polypeptide (Oatp); multiple resistance-associated protein 2 and 3 (Mrp2 and Mrp3)

DMD Fast Forward. Published on January 23, 2019 as DOI: 10.1124/dmd.118.084624
This article has not been copyedited and formatted. The final version may differ from this version.

Abstract

In the liver, several approaches are used to investigate and predict the complex issue of drug-induced transporter inhibition. These approaches include in vitro assays and pharmacokinetic models that predict how inhibitors modify the systemic and liver concentrations of the victim drugs. Imaging is another approach that shows how inhibitors might alter liver concentrations stronger than systemic concentrations. In perfused rat livers associated with a gamma counter that measures continuously liver concentrations, we previously showed how fluxes across transporters generate the hepatocyte concentrations of two clinical imaging compounds, one with a low extraction ratio (Gadobenate dimeglumine, BOPTA) and one with a high extraction ratio (Mebrofenin, MEB). BOPTA and MEB are transported by rat Oatps and Mrp2 which are both inhibited by rifampicin. The aim of the study is to measure how rifampicin modifies the hepatocyte concentrations and membrane clearances of BOPTA and MEB and to determine whether these compounds might be used to investigate transporter-mediated drug-drug interactions in clinical studies. We show that rifampicin co-perfusion greatly decreases BOPTA hepatocyte concentrations, but increases those of MEB. Rifampicin decreases strongly BOPTA hepatic clearance. In contrast, rifampicin decreases moderately MEB hepatic clearance and blocks the biliary intrinsic clearance, increasing MEB hepatocyte concentrations. In conclusion, low concentrations prevent the quantification of BOPTA biliary intrinsic clearance, while MEB is a promising imaging probe substrate to evidence transporter-mediated drug-drug interactions when inhibitors act on influx and efflux transporters.

DMD Fast Forward. Published on January 23, 2019 as DOI: 10.1124/dmd.118.084624
This article has not been copyedited and formatted. The final version may differ from this version.

Introduction

Several approaches are used to investigate and predict the complex issue of drug-induced transporter inhibition. The topic is widely described in *in vitro* assays but the translational information to patients is questioned because the inhibition is mainly tested with prototypical and not clinically relevant substrates (Belzer et al., 2013; Martinez-Guerrero and Wright, 2013; Izumi et al., 2015; Koide et al., 2017; Pedersen et al., 2017). In the liver, several pharmacokinetic models describe how transporter inhibition modifies the drug clearances across these transporters to explain and predict the modified systemic concentrations induced by inhibitors (Watanabe et al., 2010; Yoshida et al., 2012; Patilea-Vrana and Unadkat, 2016; Benet et al., 2018a; Benet et al., 2018b; Patilea-Vrana and Unadkat, 2018). Another approach of drug-induced transporter inhibition relies on liver imaging (Langer, 2016; Tournier et al., 2018). Liver imaging estimates concentrations which should be high enough for drugs targeting hepatocytes but low enough to avoid cell injury when the target is extrahepatic (Chu et al., 2013; Dollery, 2013; Guo et al., 2018). Pharmacokinetic models of liver images acquired over time estimate transfer rates and clearances between 2 compartments of the liver, as well as liver area-under-the curve (AUC_{liver}) (Ali et al., 2018; Bauer et al., 2018a; Caille et al., 2018; Kaneko et al., 2018; Leporq et al., 2018). Some of these studies suggest that liver concentrations might be more altered than systemic concentrations when inhibitors such as rifampicin are concomitantly substrates of uptake transporters and decrease bile excretion rates (Patilea-Vrana and Unadkat, 2016; Benet et al., 2018a; Kaneko et al., 2018; Patilea-Vrana and Unadkat, 2018). To detect transporter-mediated drug-drug interactions, imaging analyses whether a potential inhibitor modifies the liver distribution of a transporter-specific tracer or MR contrast agent (Langer, 2016). These compounds are designated usually as imaging probe substrates.

In perfused rat livers, we demonstrated previously how drug influx and efflux across membrane transporters generate the hepatocyte concentrations of two hepatobiliary

compounds used in clinical imaging: gadobenate dimeglumine (MultiHance®, Bracco Imaging, Milan, BOPTA) for magnetic resonance imaging (MRI) (Daali et al., 2013) and ^{99m}Tc-mebrofenin (Choletec®, Bracco Imaging, Milan) for single photon emission computed tomography (SPECT) imaging (Bonnaventure and Pastor, 2015). This experimental model was original because we placed a gamma counter over a liver lobe that measures continuously the liver concentrations of both compounds. Hepatocyte concentrations can then be calculated easily knowing the extracellular and biliary concentrations. BOPTA (Planchamp et al., 2007; Millet et al., 2011) and MEB (Ghibellini et al., 2008; de Graaf et al., 2011; Neyt et al., 2013) enter into hepatocytes through the organic anion transporting polypeptides (Oatps) and efflux from cells back to sinusoids (via the multiple resistance-associated protein 3, Mrp3) (Ghibellini et al., 2008) and into bile canaliculi (via the Mrp2) (Ghibellini et al., 2008; Millet et al., 2011) (Fig. 1). The biliary excretion rates of MEB measured in sandwich-cultured hepatocytes from rats lacking Mrp2 is negligible (Swift et al., 2010) and mice deficient in Mrp2 transporter do not excrete MEB into bile canaliculi (Neyt et al., 2013). BOPTA and MEB are not metabolised in hepatocytes and their hepatic pharmacokinetics is different because BOPTA has a low liver extraction ratio, while that of MEB is very high. With the same experimental model, we quantified the hepatic distribution of the transporter inhibitor rifampicin. When 100 µM rifampicin were perfused in rat livers, its hepatic clearance into hepatocytes at steady state was 5 ml/min and its extraction ratio was 17% (Daali et al., 2013). In this study, we quantified the liver concentrations of rifampicin by serial biopsies along the perfusion protocol. The maximal liver concentrations were 668 ± 93 µM. Rifampicin is a substrate (Tirona et al., 2003) and inhibitor of rat and human OATPS (Tirona et al., 2003; Karlgren et al., 2012). The transport of rifampicin across Mrp2 was not investigated but we showed that the rifampicin bile excretion rates are negligible in normal rats in comparison to its high basolateral efflux back to sinusoids (Daali et al., 2013).

DMD Fast Forward. Published on January 23, 2019 as DOI: 10.1124/dmd.118.084624
This article has not been copyedited and formatted. The final version may differ from this version.

The aim of the study was to measure how rifampicin modifies the hepatocyte concentrations and membrane clearances of BOPTA and MEB in our model that includes the continuously measurements of liver concentrations and to determine whether these compounds might be useful to investigate transporter-mediated drug-drug interactions in clinical studies.

Material and Methods

Animals

Before liver isolation, male Sprague-Dawley rats (n = 19) were anesthetised with pentobarbital (50 mg · kg^{-1} ip). The protocol was carried out in accordance with the Swiss Guidelines for the Care and Use of Laboratory Animals and was approved by the local animal welfare committee and the veterinary office in Geneva, Switzerland. We previously perfused 3 rats with BOPTA and rifampicin, and for this group we reanalysed the raw data to calculate the clearance parameters (Daali et al., 2013).

Isolated perfused rat livers

We isolated and perfused the rat livers as published recently (Bonnaventure and Pastor, 2015; Daire et al., 2017). The rat livers were isolated leaving organs in the carcass. The abdominal cavity was opened and the portal vein was cannulated (16 Gauge catheter). The hepatic artery was not perfused. The abdominal vena cava was transected and an oxygenated Krebs-Henseleit-bicarbonate (KHB) solution (118 mM NaCl, 1.2 mM $MgSO_4$, 1.2 mM KH_2PO_4, 4.7 mM KCl, 26 mM $NaHCO_3$, 2.5 mM $CaCl_2$) was pumped without delay into the portal vein, the solution being discarded following liver distribution by a vena cava transection. The flow rate was slowly increased over one minute up to 30 ml/min to prevent injury of sinusoidal cells. In a second step, the chest was opened and a cannula (14 Gauge) was inserted through the right atrium to collect solutions flowing from hepatic veins. Finally, the abdominal inferior vena cava was ligated allowing the KHB solutions perfused by the portal vein to be eliminated by the hepatic veins.

The perfusion system included a reservoir, a pump, a heating circulator, a bubble trap, a filter, and an oxygenator. Solutions of perfusion were equilibrated with a mixture of 95% O_2-5% CO_2. The livers were perfused with the KHB buffer ± drugs using a non-recirculating

DMD Fast Forward. Published on January 23, 2019 as DOI: 10.1124/dmd.118.084624
This article has not been copyedited and formatted. The final version may differ from this version.

system, livers being always perfused by fresh solutions. In each liver, the common bile duct was cannulated with a PE_{10} catheter and bile samples collected every 5 min to measure bile flow rates (µl/min/liver) and BOPTA and MEB concentrations (in µM). Samples were also collected from the hepatic veins (HV) each 5 min to measure BOPTA and MEB concentrations (µM).

Drug perfusion

Rat livers were perfused with either gadopentetate dimeglumine (DTPA, Magnevist®, Bayer Pharma) and gadobenate dimeglumine (BOPTA, MultiHance®, Bracco Imaging) or Technescan DTPA®, b.e.imaging, Schwyz, Switzerland (DTPA) and mebrofenin (MEB, Choletec®, Bracco Imaging). DTPA distributes within the sinusoids and the interstitium, while BOPTA and MEB enter into hepatocytes before excretion into bile canaliculi. In the first group of rats, ^{153}Gd-DTPA and ^{153}Gd-BOPTA were obtained by adding $^{153}GdCl_3$ (1 MBq/mL) to the commercially available 0.5 M solutions DTPA and BOPTA. In the second group of rats, 25 mg DTPA and MEB were labelled with ^{99m}Tc (7 and 11 MBq, respectively). Then, ^{153}Gd-DTPA and ^{153}Gd-BOPTA were diluted in the KHB solutions to obtain 200-µM concentrations, while ^{99m}Tc-DTPA and ^{99m}Tc-MEB were diluted to obtain 64-µM concentrations. The livers were successively perfused with either 200 µM ^{153}Gd-DTPA (10 min), KHB solution (35 min), 200 µM ^{153}Gd-BOPTA (perfusion period, 30 min), and KHB solution (rinse period, 30 min) or with 64 µM ^{99m}Tc-DTPA (10 min), KHB solution (35 min), 64 µM ^{99m}Tc-MEB (perfusion period, 30 min), and KHB solution (rinse period, 30 min). Thus, two periods are distinguished: 1) a perfusion period that evidences drug accumulation in liver compartments; and 2) a rinse period that investigates drug hepatocyte effluxes into bile canaliculi and back to sinusoids. The maximal perfusion period for each experiment was 105 min. DTPA is perfused to calculate the BOPTA and MEB hepatocyte concentrations (see following section).

Rats were perfused with 200 µM BOPTA (n = 6) or 64 µM MEB (n = 6) during the perfusion period. In two additional groups, BOPTA and MEB perfusion were associated with rifampicin (100 µM): BOPTA+RIF (n = 3) and MEB+RIF (n = 4) groups. Rifampicin was not perfused during the rinse period.

Quantification of drug concentrations over time in liver compartments

To quantify the liver concentrations, a gamma counter that measured count rates every 20 seconds was placed 1 cm above a liver lobe. The counter measured the radioactivity in a region-of-interest that was identical in each experiment. To transform the count rates into drug concentrations, the total liver radioactivity was measured by an activimeter (Isomed 2000, Canberra, Saint-Quentin-en-Yvelines, France) at the end of each experiment and was related to the last count rates. DTPA, BOPTA, and MEB concentrations in common bile duct and hepatic veins were measured every 5 min with a gamma counter (Camberra, Saint-Quentin-en-Yvelines, France). Concentrations are expressed in µM in great vessels, bile duct, and livers. We considered that 1 g of liver was close to 1 ml. All concentrations measured in solutions or livers ranged within standard values. Bile samples were diluted.

Calculation of hepatocyte drug concentrations

In the region-of-interest, the drug liver concentrations were the sum of the concentrations in the extracellular space, bile canaliculi, and hepatocytes. The concentrations of the extracellular space were assessed during DTPA perfusion. The concentrations in the bile canaliculi measured by the counter were calculated by multiplying the bile concentrations in the common bile duct by the volume of bile canaliculi (%) in the rat liver. Blouin et al. (Blouin et al., 1977) estimated previously this volume at 0.43%. We also assumed that the drug concentrations were similar in the bile canaliculi and the common bile

duct, although solute export from the cholangiocytes and water transport along ductules and ducts may modify the primary bile composition. The drug hepatocyte concentrations were calculated by subtracting the DTPA and bile canaliculi concentrations to the liver concentrations. Finally, because drug concentrations measured by the counter originated from a 78%-volume of hepatocytes (Blouin et al., 1977), we increased the calculated values to 100% to obtain the true concentrations in the hepatocyte volume.

Drug influx into hepatocytes

The net removal rate of drug from sinusoids (v in nmol/min) were measured by Q_H (C_{in} - C_{out}) where Q_H is the liver flow rate (30 ml/min in all experiments), C_{in} is the constant concentrations entering the liver via the portal vein, and C_{out} is the measured concentrations in hepatic veins. The unbound fraction of drugs in blood (f_B) was 1 because no protein is added into the perfusate and C_{in} and C_{out} are similar to f_B C_{in} and f_B C_{out}. The hepatic clearance (CL in ml/min) is the ratio of v and C_{in}. The drug liver extraction ratio (E) is (C_{in} – C_{out})/C_{in}.

Using the counter placed over the liver, the hepatocyte uptake into hepatocytes (in µM/min) was measured by the slope of the relation between hepatocyte concentrations and time over 2 min at the very beginning of the drug perfusion to avoid an underestimation of hepatocyte concentrations associated with early excretion into bile canaliculi. A delay of 1 min (from 45 to 46 min) assured a homogenous drug distribution within the interstitium.

Drug efflux from hepatocytes

The biliary excretion rate (v_{bile} in nmol/min) was calculated by C_{bile} x bile flow rate (Q_{bile}), where C_{bile} is the drug concentration measured in the common bile duct. The biliary intrinsic clearance ($f_L CL_{int,bile}$ in ml/min) was le ratio of v_{bile} and hepatocyte concentrations (C_{HC} in nmol/g or µM). The drug unknown fraction in liver is f_L. v_{bile} and $f_L CL_{int,bile}$ were

measured every 5 min. The basolateral efflux out of hepatocytes (v_{ef} in nmol/min) was calculated by C_{out} x Q_H and the basolateral efflux clearance (f_LCL_{ef} in ml/min) is v_{ef} divided by $C_{HC.}$ To calculate the partition of drug efflux into bile canaliculi and sinusoids, we measured the ratio of the area-under-the curves of v_{bile} and v_{ef} from 85 to 105 min ($AUCRv_{bile/}v_{ef}$). V_{ef} is not available during the perfusion period because, in hepatic veins, we cannot distinguish between the drugs that returned from hepatocytes into sinusoids from those that never entered into hepatocytes. However, knowing f_LCL_{ef}, we can extrapolate drug concentrations that efflux through Mrp3 (C_{Mrp3}) at the end of the perfusion period (T75 min): $C_{Mpr3,75min}$ = $f_LCL_{ef} \cdot C_{HC,75min} / Q_H$. We can then calculate $f_L\ CL_{in,75min} = (C_{in} - C_{out} - C_{Mrp3,75min})\ Q_H/C_{in}$.

Inhibition potency of rifampicin on systemic and hepatocyte MEB and BOPTA concentrations

To better quantify the inhibition potency of rifampicin on systemic and hepatocyte drug concentrations, we calculated the AUC of hepatocyte concentrations ($AUC_{HC,45-105}$) from 45 to 105 min and C_{out} ($AUC_{Cout,45-75}$) from 45 to 75 min in the 4 experimental groups and determined the following ratios: $AUCR_{HC,+RIF/-RIF}$ and $AUCR_{Cout,+RIF/-RIF}$. Indeed, in our model, C_{out} changes estimate those of the systemic circulation.

Viability of liver perfusion

Liver viability during the experimental period (105 min) was assessed by measuring portal pressures and bile flow rates. The portal pressures remained < 10 mmHg in all rats. In the absence of red blood cells in the perfusate, we (Pastor et al., 1998) and other researchers (Mischinger et al., 1992) used a flow rate of 3 ml/min/g of liver. With such flow rate, portal pressures remained steady in the 4 groups of rats: 4.7 ± 0.4 mmHg (BOPTA); 5.8 ± 1.0 mmHg (BOPTA+RIF); 7.7 ± 1.2 mmHg (MEB); 8.0 ± 1.0 mm Hg (MEB+RIF). This flow rate delivers enough O_2 to maintain a normal liver O_2 consumption (Pastor et al., 1998). It also prevents the inhomogeneous distribution of perfused solutions (Bessems et al., 2006).

A steady bile flow is another parameter of liver viability during the experimental protocol. Bile flow rates were measured in the 4 experimental groups over time (Fig. 2).

Statistics

Parameters are means ± S.D. To compare the evolution of parameters over time in one group, we use a one-way ANOVA and to compare parameters over time in several groups, we use a two-way ANOVA with the Sidak's multiple comparison test of mean values at each time-point between groups (Prism 7, GraphPad, La Jolla, CA, USA). To analyse the drug uptake rates over time and the relationship between bile excretion rates and bile concentrations, we used linear regressions.

Results

Effect of drugs on liver flow rates

BOPTA is a choleretic drug. Bile flow rates increased during the perfusion and recovered along the rinse period (Fig. 2). MEB perfusion had no effect on bile flow rates and rifampicin perfusion decreased slightly the bile flow rates with a rapid recovery before the end of the protocol. Thus, only BOPTA bile excretion rates relied on both increased canalicular fluid transfer and biliary concentrations.

MEB and BOPTA hepatic pharmacokinetics and concentrations

The MEB removal rate from sinusoids (v) was steady over time (1797 ± 61 nmol/min) and the maximal bile excretion rate (v_{bile}) reached 990 ± 166 nmol/min at the end of the perfusion period (Fig. 3C, right *Y-axis*). The MEB basolateral efflux from hepatocytes ($v_{ef,85-105}$) was measured during the rinse period because during this period MEB C_{out} originated only from hepatocytes. The efflux was minimal (< 10 nmol/min). These three fluxes generated an increase in hepatocyte concentrations over time that reached 2611 ± 98 µM (Fig. 3B). The low concentrations in hepatic veins (C_{out}) around 4 µM (Fig. 3A), explained the high extraction ratio of MEB (0.93 ± 0.03).The maximal bile concentration was 97'017 ± 11'289 µM (Fig. 3C, left *Y-axis*). During the rinse period, all parameters decreased steadily in the absence of MEB perfusion.

The BOPTA removal rate from sinusoids (v) was much lower than that of MEB and significantly decreased over time to reach a steady value of 464 ± 80 nmol/min. C_{out} were close to C_{in} (Fig. 4A), and the liver extraction ratio was 0.08 ± 0.01. The maximal bile excretion rate (Fig. 4C, right *Y-axis*) and the bile concentrations (Fig. 4C, *X-axis*) were lower during BOPTA perfusion in comparison to MEB perfusion ($p < 0.0001$). The ratio of $AUCv_{bile}$ and $AUCv_{ef}$ ($AUCRv_{bile/v_{ef}}$) from 85 to 105 min were 5.3 (BOPTA) and 40.4 (MEB). Thus,

MEB basolateral efflux was negligible and only BOPTA v_{ef} might increase C_{out} measured in hepatic veins.

MEB hepatic clearance (CL) over time was steady over the perfusion period (28.2 ± 0.9 ml/min, *P* = 0.12) and much higher than BOPTA CL which decreased significantly over time to 2.5 ± 0.1 ml/min (*P* = 0.04, Fig. 3D and Fig. 4D). BOPTA and MEB f_L $CL_{int,bile}$ were steady from 55 to 75 min (Fig. 3F and Fig 4F) but values were higher in livers perfused by BOPTA (0.85 ± 0.25 ml/min) than in those perfused with MEB (0.41 ± 0.11 ml/min, *P* < 0.001). Another way to assess $CL_{int,bile}$ is to plot bile excretion rates and hepatocyte concentrations during the perfusion period (Fig. 5B). The slopes of the linear regressions were not significantly different: 0.31 ± 0.07 ml/min (MEB) and 0.66 ± 0.15 (BOPTA), *P* = 0.22. MEB f_L CL_{ef} represented only 2% of f_L $CL_{int,bile}$ (Fig. 3E and Fig. 3F), while BOPTA f_L CL_{ef} represented less than 15 % of f_L $CL_{int,bile}$ (Fig. 4E and Fig. 4F). Moreover, BOPTA f_L CL_{ef} was not steady and decreased along the rinse period. The estimated C_{Mrp3} at T75 min were 2.45 ± 0.43 µM (BOPTA) and 0.88 ± 0.18 µM (MEB). As expected, f_L CL_{in} was close to CL for MEB but higher for BOPTA (Table 1). The ratios f_L CL_{in} /CL were 1.16 (BOPTA) and 1.01 (MEB).

Two other parameters can be calculated with the experimental model. The hepatocyte uptake into hepatocytes (in µM/min) measured by the slope of the relation between hepatocyte concentrations and time over 2 min was significantly higher with MEB than with BOPTA (Fig. 5A) (P < 0.0001). The concentrative activity of Mrp2 was estimated by calculating the concentration gradients between bile and hepatocytes ($C_{bile,75min}/C_{HC,75min}$, Table 1). Both gradients were similar at 75 min (*P* = 0.92).

Effects of transporter inhibition by rifampicin

Rifampicin had very different effects on MEB and BOPTA hepatocyte concentrations. The maximal MEB hepatocyte concentrations were higher in the presence of rifampicin

(5044 ± 693 vs. 2611 ± 98 µM), while those of BOPTA were much lower (23 ± 19 vs. 566 ± 99 µM (Table 1). Thus, rifampicin impeded BOPTA entry into hepatocytes, and the hepatocyte uptake from 46 to 48 min was only 3 ± 3 µM/min (Fig. 5A). Consequently, BOPTA hepatocyte concentrations became too low to analyse correctly the inhibitory effect of rifampicin on Mrp2. MEB hepatocyte uptake was moderately lower in the presence (210 ± 3 µM/min) than in the absence (296 ± 1 µM/min) of rifampicin ($P < 0.0001$, Fig. 5A) and the concomitant Mrp2 inhibition by rifampicin increased MEB hepatocyte concentrations over time.

BOPTA hepatocyte concentrations over time (AUC_{HC}) found similar results. AUC_{HC} were 18'822 ± 3'758 µM.min (BOPTA) and 1'174 ± 440 µM.min (BOPTA+RIF) ($P = 0.02$) with a ratio of 0.47. AUC_{HC} were 90'564 ± 17'933 µM.min (MEB) and 180'203 ± 21'308 µM.min (MEB+RIF) ($P = 0.01$) with a ratio of 2. The higher MEB and BOPTA concentrations in hepatic veins in the presence of the inhibitor confirmed the decreased MEB entry into hepatocytes (Fig. 3A and Fig. 4A) as did $AUC_{Cout,45\text{-}75}$. The ratio $AUCR_{Cout}$ was 1.07: 4'503 ± 71 µM.min (BOPTA) and 4'820 ± 38 µM.min (BOPTA+RIF) ($P = 0.02$). MEB $AUCR_{Cout}$ was 6.43: 110 ± 47 µM.min (MEB) and 708 ± 117 µM.min (MEB+RIF), ($P = 0.01$).

During rifampicin perfusion, MEB bile excretion rate was blocked with a recovery along the rinse period (Fig. 3C, left *Y-axis*). The effect of rifampicin (+RIF/-RIF ratios, Table 1) was higher for v_{bile} (0.11) and $CL_{int,bile}$ (0.05) than for v (0.57) and CL_{in} (0.55). The effect of rifampicin on MEB $f_L CL_{ef}$ were too low to draw a conclusion.

Discussion

Our study shows that MEB is a promising imaging probe substrate to evidence the transporter-mediated drug-drug interactions when inhibitors such as rifampicin act on influx and efflux transporters. In the presence of 100 µM rifampicin, the decline of CL_{in} depletes hepatocytes from BOPTA at such low level that Mrp2 inhibition is difficult to detect. The low extraction ratio of BOPTA might be a disadvantage for such preclinical investigations. However, in a similar protocol, we showed previously that the BOPTA hepatocyte uptake increases slightly by decreasing the rifampicin concentrations from 100 µM to 1 µM (Daali et al., 2013). MEB hepatocyte uptake was decreased moderately in the presence of rifampicin and the concomitant Mrp2 inhibition by rifampicin increased MEB hepatocyte concentrations over time. The hepatocyte concentrations-time curve ratios $AUCR_{HC,+RIF/-RIF}$ were divergent: 0.47 (BOPTA) and 2 (MEB). Rifampicin increased C_{out} measured in hepatic veins for both imaging compounds and the hepatic vein concentrations-time curve ratios $AUCR_{Cout,+RIF/-RIF}$ increased: 1.07 (BOPTA) and 6.43 (MEB).

In volunteers, MEB was previously injected with the HIV protease inhibitor Ritonavir which is a substrate and inhibitor of both Oatps and Mrp2 in experimental models (Pfeifer et al., 2013). The MEB systemic concentrations significantly increased while liver and bile concentrations did not change. This study confirms the interest of the imaging probe substrate to investigate transporter-drug-drug interactions in humans. Additional results were obtained with Positron Emission Tomography (PET) probe substrates in the presence of rifampicin (Bauer et al., 2018b; Kaneko et al., 2018). MEB was also used as an imaging probe substrate by Ali et al. (Ali et al., 2018) to determine the OATP and MRP2 functions in patients with nonalcoholic fatty liver disease. The liver disease decreases both MEB CL_{in} and $CL_{int,bile}$ with increased liver and systemic concentrations over time.

Our experimental model also shows that fluxes across transporters generate the hepatocyte concentrations over time. Moreover, it enables an independent quantification of hepatocyte concentrations while Benet et al. (Benet et al., 2018b) highlighted recently the difficulty to obtain such values. Consequently, true biliary intrinsic clearances over time were calculated independently of the hepatocyte uptake. These biliary intrinsic clearances were measured over time and by calculating the slopes of the relationship between bile excretion rates and hepatocyte concentrations. BOPTA clearances are higher than MEB clearances but statistical significance is obtained only when values are measured over time. In the presence of rifampicin, the MEB biliary intrinsic clearance is significantly decreased.

Besides the biliary intrinsic clearance, we calculated the basolateral influx and efflux clearances to characterise the rate-limiting step of the systemic clearances. MEB f_L CL_{ef} represents 2% of f_L $CL_{int,bile}$ while BOPTA f_L CL_{ef} represented less than 15 % of f_L $CL_{int,bile}$. Thus, MEB basolateral efflux was negligible as previously published in human livers (Ghibellini et al., 2008) and only BOPTA increases C_{out} with CL_{in} values higher than hepatic CL. Consequently, both imaging compounds have $CL_{in} > CL_{int,bile} \gg CL_{ef}$. However, clearances measured over time are not steady. Biliary intrinsic clearances increase at the beginning of the perfusion and rinse periods. This time-dependence might be attributed to the changes of perfusion solutions that may induce an inhomogeneous drug distribution within sinusoids. The decreased clearances during the rinse period might be associated with an inhomogeneity of drug concentrations within each hepatocyte where drugs disappear around the sinusoidal membrane while drug concentrations are maintained around the canalicular membrane. The crosstalk between both membranes might be lost. However, these comments remain speculative. The hepatic clearances are steady over time for MEB but decrease to a steady state with BOPTA.

Finally, the gradient of bile and hepatocyte concentrations over time quantifies the Mrp2 activity which is similar for BOPTA and MEB. The parameters decrease greatly in the

DMD Fast Forward. Published on January 23, 2019 as DOI: 10.1124/dmd.118.084624
This article has not been copyedited and formatted. The final version may differ from this version.

presence of rifampicin. Interesting, these parameters are available in liver imaging (Takashima et al., 2012; Kaneko et al., 2018) and might detect drug-induced liver toxicity in humans.

The isolated and perfused rat liver is a convenient model because the experimental conditions are well controlled and simplified. However, livers are perfused only through the portal vein, avoiding the complexity of a dual input entry, a condition that can change the physiological liver perfusion. The imaging compounds we use are free to enter into hepatocytes because the perfused solutions do not contain protein and f_B in perfusate is 1, but in the bile and liver, the compounds bind to proteins and the counter is unable to discriminate their free and bound fractions. Consequently, except for CL_{in} (with f_B = 1), clearances are expressed as f_L CL_{ef} and f_L $CL_{int,bile}$. The gamma counter placed over the liver detects the concentrations of both imaging compounds, avoiding the collection of serial liver biopsies. Indeed, serial biopsies alter the liver structure over the protocol (Cusin et al., 2017). This improved experimental model measures directly the effects of rifampicin on fluxes across hepatocyte membranes and is a new tool for the understanding of transporter-mediated drug-drug interactions. We can measure or calculate the concentrations in all liver compartments, except within the interstitium. It describes with precision the drug behaviour in rat livers and might validate the data obtained by pharmacokinetic analysis and simulations (Watanabe et al., 2010; Yoshida et al., 2012; Patilea-Vrana and Unadkat, 2016; Benet et al., 2018a; Benet et al., 2018b; Patilea-Vrana and Unadkat, 2018).

Authorship contributions

Participated in research design: Pierre Bonnaventure, Catherine M Pastor

Conducted experiments: Pierre Bonnaventure, Fabien Cusin

Performed data analysis: Pierre Bonnaventure, Fabien Cusin, Catherine M Pastor

Wrote or contributed to the writing of the manuscript: Pierre Bonnaventure, Fabien Cusin, Catherine M Pastor

References

Ali I, Slizgi JR, Kaullen JD, Ivanovic M, Niemi M, Stewart PW, Barritt ASt, and Brouwer KLR (2018) Transporter-mediated alterations in patients with NASH increase systemic and hepatic exposure to an OATP and MRP2 substrate. *Clin Pharmacol Ther* **104:**749-756.

Bauer M, Matsuda A, Wulkersdorfer B, Philippe C, Traxl A, Ozvegy-Laczka C, Stanek J, Nics L, Klebermass EM, Poschner S, Jager W, Patik I, Bakos E, Szakacs G, Wadsak W, Hacker M, Zeitlinger M, and Langer O (2018a) Influence of OATPs on hepatic disposition of Erlotinib measured with Positron Emission Tomography. *Clin Pharmacol Ther* **104:**139-147.

Bauer M, Traxl A, Matsuda A, Karch R, Philippe C, Nics L, Klebermass EM, Wulkersdorfer B, Weber M, Poschner S, Tournier N, Jager W, Wadsak W, Hacker M, Wanek T, Zeitlinger M, and Langer O (2018b) Effect of rifampicin on the distribution of [(11)C]Erlotinib to the liver, a translational PET study in humans and in mice. *Mol Pharm* **15:**4589-4598.

Belzer M, Morales M, Jagadish B, Mash EA, and Wright SH (2013) Substrate-dependent ligand inhibition of the human organic cation transporter OCT2. *J Pharmacol Exp Ther* **346:**300-310.

Benet LZ, Bowman CM, Liu S, and Sodhi JK (2018a) The Extended Clearance concept following oral and intravenous dosing: theory and critical analyses. *Pharm Res* **35:**242.

Benet LZ, Liu S, and Wolfe AR (2018b) The universally unrecognized assumption in predicting drug clearance and organ extraction ratio. *Clin Pharmacol Ther* **103:**521-525.

Bessems M, t Hart NA, Tolba R, Doorschodt BM, Leuvenink HG, Ploeg RJ, Minor T, and van Gulik TM (2006) The isolated perfused rat liver: standardization of a time-honoured model. *Lab Anim* **40:**236-246.

Blouin A, Bolender RP, and Weibel ER (1977) Distribution of organelles and membranes between hepatocytes and nonhepatocytes in the rat liver parenchyma. A stereological study. *The Journal of cell biology* **72:**441-455.

Bonnaventure P and Pastor CM (2015) Quantification of drug transport function across the multiple resistance-associated protein 2 (Mrp2) in rat livers. *Int J Mol Sci* **16:**135-147.

Caille F, Goutal S, Marie S, Auvity S, Cisternino S, Kuhnast B, Pottier G, and Tournier N (2018) Positron Emission Tomography imaging reveals an importance of saturable liver uptake transport for the pharmacokinetics of metoclopramide. *Contrast Media Mol Imaging* **2018:**7310146.

Chu X, Korzekwa K, Elsby R, Fenner K, Galetin A, Lai Y, Matsson P, Moss A, Nagar S, Rosania GR, Bai JP, Polli JW, Sugiyama Y, and Brouwer KL (2013) Intracellular drug

concentrations and transporters: measurement, modeling, and implications for the liver. *Clin Pharmacol Ther* **94:**126-141.

Cusin F, Fernandes Azevedo L, Bonnaventure P, Desmeules J, Daali Y, and Pastor CM (2017) Hepatocyte concentrations of Indocyanine Green reflect transfer rates across membrane transporters. *Basic Clin Pharmacol Toxicol* **120:**171-178.

Daali Y, Millet P, Dayer P, and Pastor CM (2013) Evidence of drug-drug interactions through uptake and efflux transport systems in rat hepatocytes: implications for cellular concentrations of competing drugs. *Drug Metab Dispos* **41:**1548-1456.

Daire JL, Leporq B, Vilgrain V, Van Beers BE, Schmidt S, and Pastor CM (2017) Liver perfusion modifies Gd-DTPA and Gd-BOPTA hepatocyte concentrations through transfer clearances across sinusoidal membranes. *Eur J Drug Metab Pharmacokinet* **42:**657-667.

de Graaf W, Hausler S, Heger M, van Ginhoven TM, van Cappellen G, Bennink RJ, Kullak-Ublick GA, Hesselmann R, van Gulik TM, and Stieger B (2011) Transporters involved in the hepatic uptake of (99m)Tc-mebrofenin and indocyanine green. *J Hepatol* **54:**738-745.

Dollery CT (2013) Intracellular drug concentrations. *Clin Pharmacol Ther* **93:**263-266.

Ghibellini G, Leslie EM, Pollack GM, and Brouwer KL (2008) Use of tc-99m mebrofenin as a clinical probe to assess altered hepatobiliary transport: integration of in vitro, pharmacokinetic modeling, and simulation studies. *Pharm Res* **25:**1851-1860.

Guo Y, Chu X, Parrott NJ, Brouwer KLR, Hsu V, Nagar S, Matsson P, Sharma P, Snoeys J, Sugiyama Y, Tatosian D, Unadkat JD, Huang SM, Galetin A, and International Transporter C (2018) Advancing predictions of tissue and intracellular drug concentrations using in vitro, imaging and PBPK modeling approaches. *Clin Pharmacol Ther* **104:**865-889.

Izumi S, Nozaki Y, Maeda K, Komori T, Takenaka O, Kusuhara H, and Sugiyama Y (2015) Investigation of the impact of substrate selection on in vitro organic anion transporting polypeptide 1B1 inhibition profiles for the prediction of drug-drug interactions. *Drug Metab Dispos* **43:**235-247.

Kaneko K, Tanaka M, Ishii A, Katayama Y, Nakaoka T, Irie S, Kawahata H, Yamanaga T, Wada Y, Miyake T, Toshimoto K, Maeda K, Cui Y, Enomoto M, Kawamura E, Kawada N, Kawabe J, Shiomi S, Kusuhara H, Sugiyama Y, and Watanabe Y (2018) A clinical quantitative evaluation of hepatobiliary transport of [(11)C]Dehydropravastatin in humans using Positron Emission Tomography. *Drug Metab Dispos* **46:**719-728.

Karlgren M, Vildhede A, Norinder U, Wisniewski JR, Kimoto E, Lai Y, Haglund U, and Artursson P (2012) Classification of inhibitors of hepatic organic anion transporting polypeptides (OATPs): influence of protein expression on drug-drug interactions. *J Med Chem* **55:**4740-4763.

Kock K and Brouwer KL (2012) A perspective on efflux transport proteins in the liver. *Clin Pharmacol Ther* **92:**599-612.

Koide H, Tsujimoto M, Takeuchi A, Tanaka M, Ikegami Y, Tagami M, Abe S, Hashimoto M, Minegaki T, and Nishiguchi K (2017) Substrate-dependent effects of molecular-targeted anticancer agents on activity of organic anion transporting polypeptide 1B1. *Xenobiotica***:**1-13.

Langer O (2016) Use of PET imaging to evaluate transporter-mediated drug-drug interactions. *J Clin Pharmacol* **56 Suppl 7:**S143-S156.

Leporq B, Daire JL, Pastor CM, Deltenre P, Sempoux C, Schmidt S, and Van Beers B (2018) Quantification of hepatic perfusion and hepatocyte function with dynamic gadoxetic acid-enhanced MRI in patients with chronic liver disease. *Clin Sci* **132:**813-824.

Martinez-Guerrero LJ and Wright SH (2013) Substrate-dependent inhibition of human MATE1 by cationic ionic liquids. *J Pharmacol Exp Ther* **346:**495-503.

Millet P, Moulin M, Stieger B, Daali Y, and Pastor CM (2011) How organic anions accumulate in hepatocytes lacking Mrp2: evidence in rat liver. *J Pharmacol Exp Ther* **336:**624-632.

Mischinger HJ, Walsh TR, Liu T, Rao PN, Rubin R, Nakamura K, Todo S, and Starzl TE (1992) An improved technique for isolated perfusion of rat livers and an evaluation of perfusates. *J Surg Res* **53:**158-165.

Neyt S, Huisman MT, Vanhove C, De Man H, Vliegen M, Moerman L, Dumolyn C, Mannens G, and De Vos F (2013) In vivo visualization and quantification of (Disturbed) Oatp-mediated hepatic uptake and Mrp2-mediated biliary excretion of 99mTc-mebrofenin in mice. *J Nucl Med* **54:**624-630.

Pastor CM, Morel DR, and Billiar TR (1998) Oxygen supply dependence of urea production in the isolated perfused rat liver. *Am J Respir Crit Care Med* **157:**796-802.

Patilea-Vrana G and Unadkat JD (2016) Transport vs. metabolism: what determines the pharmacokinetics and pharmacodynamics of drugs? Insights from the Extended Clearance Model. *Clin Pharmacol Ther* **100:**413-418.

Patilea-Vrana GI and Unadkat J (2018) When does the rate-determining step in the hepatic clearance of a drug switch from sinusoidal uptake to all hepatobiliary clearances? Implications for predicting drug-drug interactions. *Drug Metab Dispos* **46:**1487-1496.

Pedersen JM, Khan EK, Bergstrom CAS, Palm J, Hoogstraate J, and Artursson P (2017) Substrate and method dependent inhibition of three ABC-transporters (MDR1, BCRP, and MRP2). *Eur J Pharm Sci* **103:**70-76.

Pfeifer ND, Goss SL, Swift B, Ghibellini G, Ivanovic M, Heizer WD, Gangarosa LM, and Brouwer KL (2013) Effect of ritonavir on 99mTechnetium-mebrofenin disposition in humans: a semi-PBPK modeling and in vitro approach to predict transporter-mediated DDIs. *CPT Pharmacometrics Syst Pharmacol* **2:**e20.

Planchamp C, Hadengue A, Stieger B, Bourquin J, Vonlaufen A, Frossard JL, Quadri R, Becker CD, and Pastor CM (2007) Function of both sinusoidal and canalicular transporters controls the concentration of organic anions within hepatocytes. *Mol Pharmacol* **71:**1089-1097.

Swift B, Yue W, and Brouwer KL (2010) Evaluation of (99m)technetium-mebrofenin and (99m)technetium-sestamibi as specific probes for hepatic transport protein function in rat and human hepatocytes. *Pharm Res* **27:**1987-1998.

Takashima T, Kitamura S, Wada Y, Tanaka M, Shigihara Y, Ishii H, Ijuin R, Shiomi S, Nakae T, Watanabe Y, Cui Y, Doi H, Suzuki M, Maeda K, Kusuhara H, Sugiyama Y, and Watanabe Y (2012) PET imaging-based evaluation of hepatobiliary transport in humans with (15R)-11C-TIC-Me. *J Nucl Med* **53:**741-748.

Tirona RG, Leake BF, Wolkoff AW, and Kim RB (2003) Human organic anion transporting polypeptide-C (SLC21A6) is a major determinant of rifampin-mediated pregnane X receptor activation. *J Pharmacol Exp Ther* **304:**223-228.

Tournier N, Stieger B, and Langer O (2018) Imaging techniques to study drug transporter function in vivo. *Pharmacol Ther* **189:**104-122.

Watanabe T, Kusuhara H, and Sugiyama Y (2010) Application of physiologically based pharmacokinetic modeling and clearance concept to drugs showing transporter-mediated distribution and clearance in humans. *J Pharmacokinet Pharmacodyn* **37:**575-590.

Yoshida K, Maeda K, and Sugiyama Y (2012) Transporter-mediated drug--drug interactions involving OATP substrates: predictions based on in vitro inhibition studies. *Clin Pharmacol Ther* **91:**1053-1064.

Footnotes

This work was supported by the Swiss National Foundations [Grant 126030].

Legends for figures

Fig. 1. BOPTA and MEB transport across hepatocyte membranes and concentrations inside liver compartments. BOPTA and MEB distribute into sinusoids and interstitium before entry into normal hepatocytes across organic anion transporting polypeptides (Oatps). Once inside hepatocytes, both compounds exit into bile canaliculi across the multiple resistance-associated protein 2 (Mrp2) or back into sinusoids across Mrp3 transporters. Basolateral influx clearance (CL_{in}, ml/min), biliary intrinsic clearance ($CL_{int,bile}$), and efflux clearance back into sinusoids generate concentrations which increase from sinusoids, to hepatocytes and bile canaliculi (illustrated by the number of circles). Rifampicin is a substrate of Oatps and inhibits both Oatps and Mrp2. Portal vein (PV) and hepatic vein (HV).

Fig. 2. Effects of drug perfusion on bile flow rates over the experimental protocol (105 min). Livers were perfused with 200 µM BOPTA (white circles), 64 µM MEB (black squares), 200 µM BOPTA and 100 µM rifampicin (blue circles), and 64 µM MEB and 100 µM rifampicin (pink squares).

Fig. 3. MEB hepatic pharmacokinetics and concentrations. Concentrations in portal vein (C_{in}, A, black circles), hepatic veins (C_{out}, A, squares), hepatocytes (B) and bile were used to calculate the hepatic clearance (CL, D), the efflux clearance back to sinusoids (f_L CL_{ef}, E) and the biliary intrinsic clearance (f_L $CL_{int,bile}$, F). In C (right *Y-axis*), the bile excretion rates are shown for MEB (green squares) and MEB+RIF (purple squares). In sinusoids, the MEB unbound fraction was equal to 1 because no protein was added in the perfusate, while the MEB unbound fraction (f_L) was unknow in livers. Livers were perfused with 64 µM MEB (black squares) or 64 µM MEB and 100 µM rifampicin (white squares). To compare the

parameters over time, we use a two-way ANOVA with the Sidak's multiple comparison test of mean values at each time-point between groups.

Fig. 4. BOPTA hepatic pharmacokinetics and concentrations. Concentrations in portal vein (C_{in}, A, black circles), hepatic veins (C_{out}, A, squares), hepatocytes (B) and bile were used to calculate the hepatic clearance (CL, D), the efflux clearance back to sinusoids (f_L CL_{ef}, E) and the biliary intrinsic clearance (f_L $CL_{int,bile}$, F). In C (right *Y-axis*), the bile excretion rates are shown for BOPTA (green squares) and BOPTA+RIF (purple squares). In sinusoids, the BOPTA unbound fraction was equal to 1 because no protein was added in the perfusate, while the BOPTA unbound fraction (f_L) was unknow in livers. Livers were perfused with 64 µM BOPTA (black squares) or 64 µM MEB and 100 µM rifampicin (white squares). To compare the parameters over time, we use a two-way ANOVA with the Sidak's multiple comparison test of mean values at each time-point between groups.

Fig. 5. A. Using the counter placed over the liver, the hepatocyte uptake into hepatocytes (µM/min) was measured by the slope of the relation between hepatocyte concentrations and time over 2 min at the very beginning of the drug perfusion to avoid an underestimation of hepatocyte concentrations associated with early excretion into bile canaliculi. A delay of 1 min (from 45 to 46 min) assured a homogenous drug distribution within the interstitium. B. Relationship between bile excretion rates and hepatocyte concentrations. Each symbol illustrates one time-point and 6 symbols were included by liver (every 5 min between 50 and 75 min) and the slope of the linear regression obtained in each group is the biliary intrinsic clearance. Livers were perfused with 200 µM BOPTA (white circles), 64 µM MEB (black squares), 200 µM BOPTA and 100 µM rifampicin (blue circles), and 64 µM MEB and 100 µM rifampicin (pink squares).

Table 1. BOPTA and MEB pharmacokinetic parameters and concentrations in the presence (+RIF) and absence (-RIF) of rifampicin

Parameters	BOPTA	BOPTA+RIF	Ratio +RIF/-RIF	MEB	MEB+RIF	Ratio +RIF/-RIF
C_{in} (µM)	200	200		64	64	
$C_{out,75min}$ (µM)	185 ± 3	196 ± 2	1.06	5 ± 2	31 ± 4	6.2
$C_{HC,75min}$ (µM)	566 ± 99	23 ± 19	0.04	2611 ± 498	5044 ± 693	1.93
$C_{bile,75min}$ (µM)	16'791 ± 2'085	92 ± 44	0.0005	97'017 ± 11289	13'258 ± 8'363	0.14
$C_{bile,75min}/C_{HC,75min}$	30.6 ± 7.5	3.5 ± 2.9	0.11	38.4 ± 8.8	2.6 ± 1.6	0.07
v_{75min} (nmol/min)[a]	464 ± 80	111 ± 47	0.24	1797 ± 61	1022 ± 113	0.57
CL (ml/min)[b]	2.32 ± 0.40	0.56 ± 0.24	0.24	28.12 ± 0.22	15.64 ± 1.77	0.56
E[c]	0.08 ± 0.01	0.02 ± 0.01	0.25	0.93 ± 0.03	0.53 ± 0.06	0.57
$v_{bile,75min}$ (nmol/min)[d]	390 ± 84	1 ± 1	0.003	990 ± 166	105 ± 65	0.11
f_L $CL_{int,bile}$ (ml/min)[e]	0.72 ± 0.23	0.04 ± 0.03	0.06	0.39 ± 0.11	0.02 ± 0.01	0.05
f_L CL_{ef} (ml/min)[f]	0.13 - 0.07[g]	0.41 - 0.00[g]	-	0.01 ± 0.01	0.01 ± 0.01	-
f_B CL_{in} (ml/min)	2.69 ± 0.37	0.60 ± 0.20	0.22	28.54 ± 0.27	15.64 ± 1.77	0.55

Perfused drug concentration in portal vein (C_{in}); Concentration in hepatic veins (C_{out}); Hepatocyte concentration (C_{HC}); Bile concentration (C_{bile}); Drug unbound fraction in blood and liver (f_B and f_L). [a] Drug removal rate from sinusoids (v) = $Q_H \cdot (C_{in}-C_{out})$. [b] Hepatic clearance (CL): $Q_H \cdot (C_{in}-C_{out})/C_{in}$. [c] Extraction ratio (E) = $C_{in}-C_{out}/C_{in}$. [d] Bile excretion rate (v_{bile}) = $Q_{bile} \cdot C_{bile}$. [e] Biliary intrinsic clearance ($f_L \cdot CL_{int,bile}$) = v_{bile}/C_{HC}. [f] Efflux clearance back to sinusoids ($f_L \cdot CL_{ef}$) = v_{ef}/C_{HC}, with $v_{ef} = Q_H \cdot C_{out}$. [g] Mean ranges over time.

Fig. 1

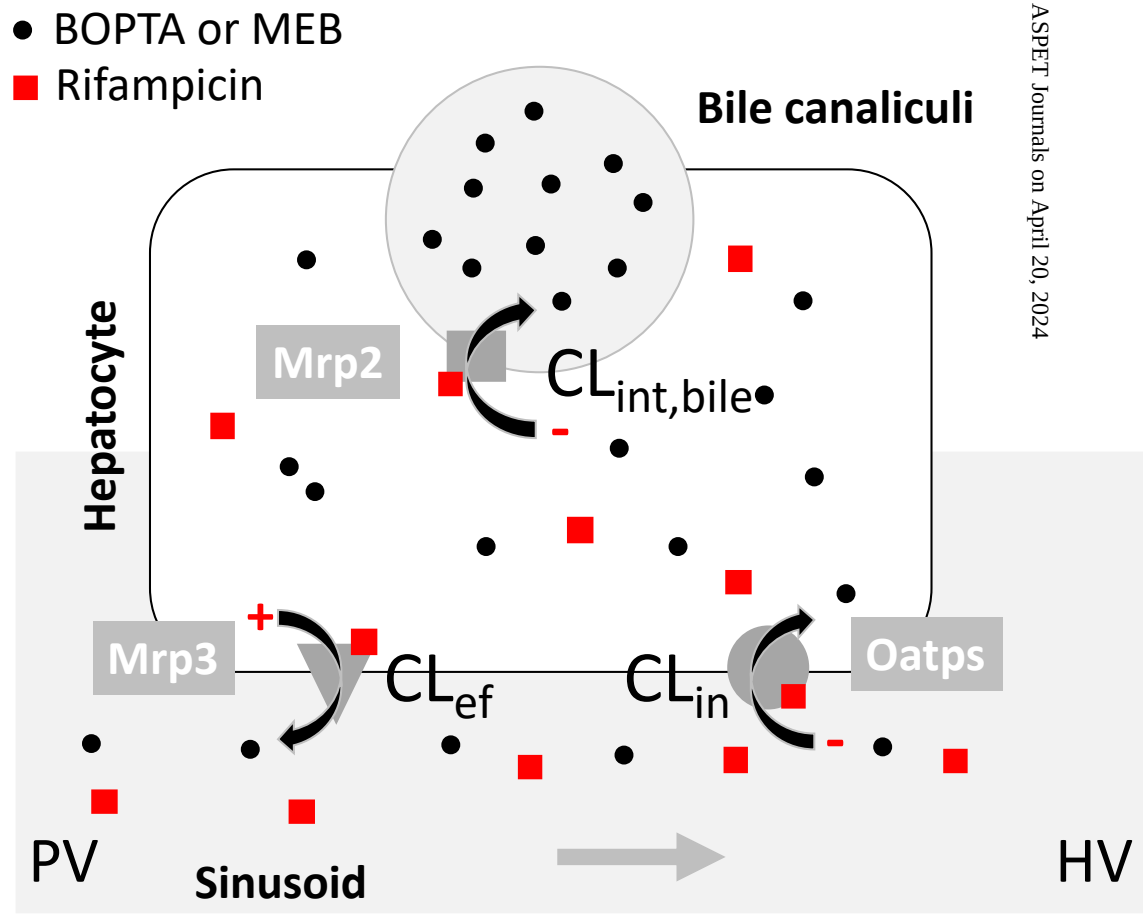

Fig. 2

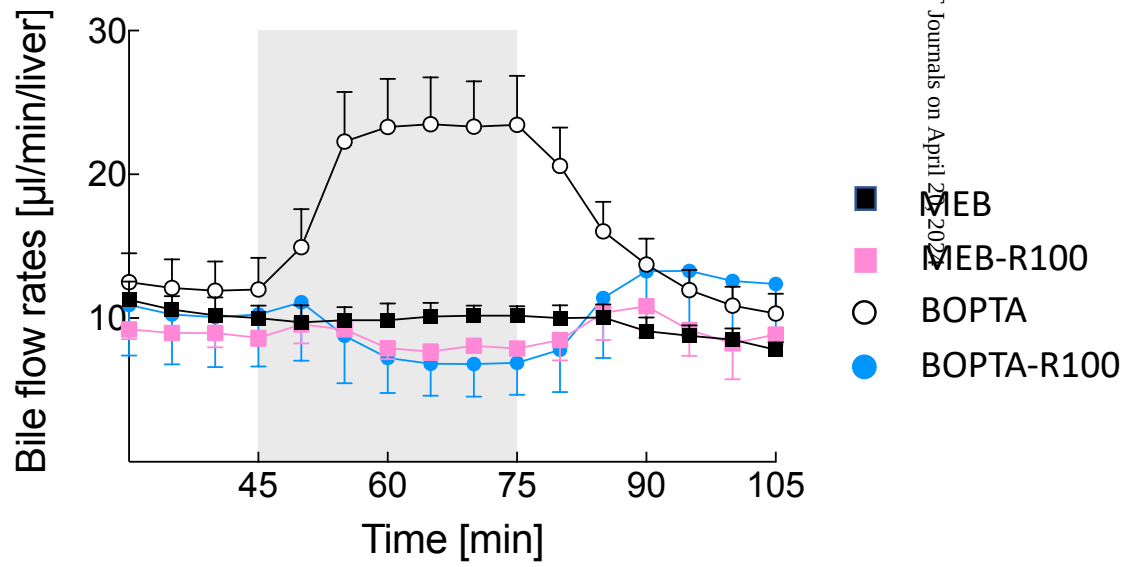

Fig. 3

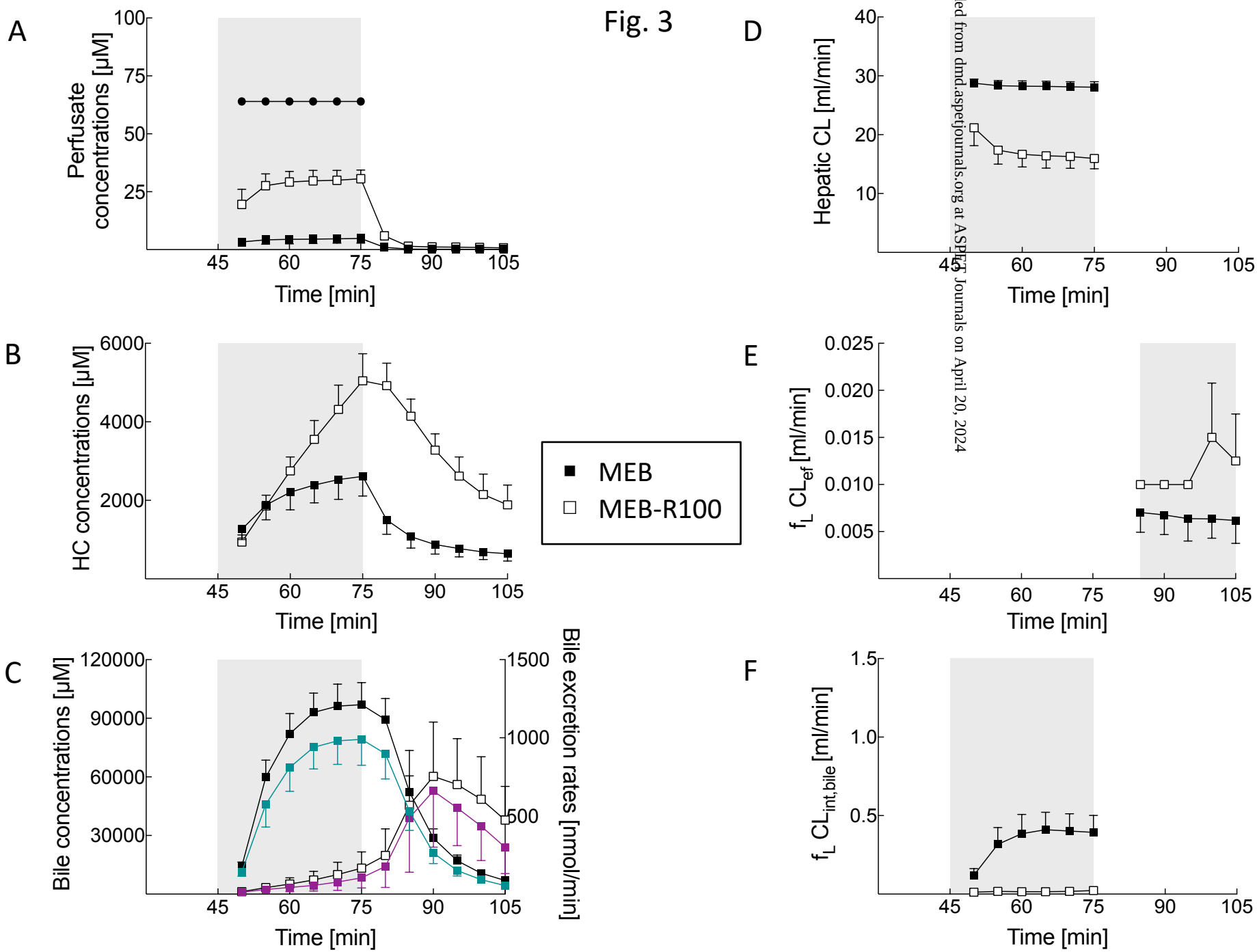

Fig. 4

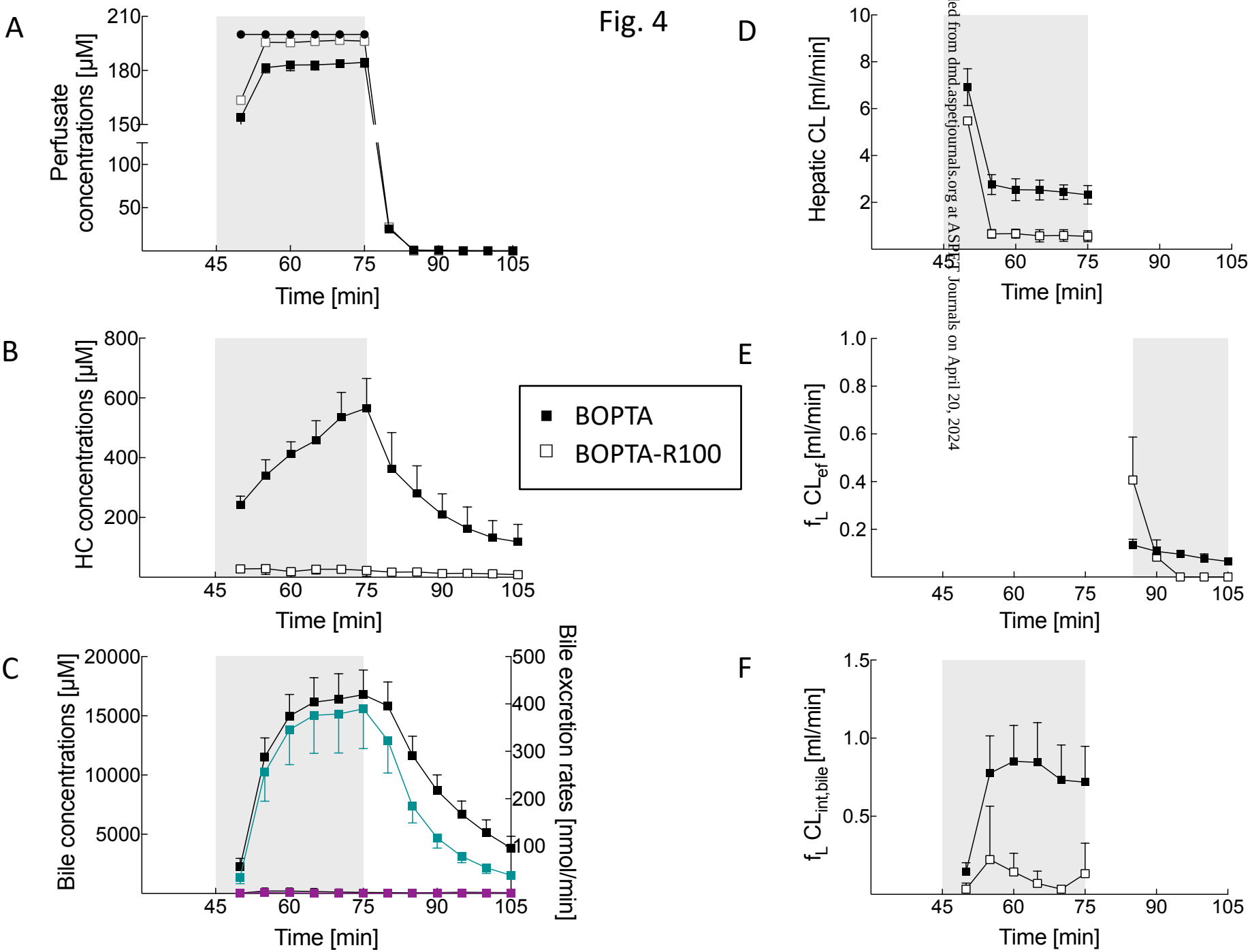

Fig. 5

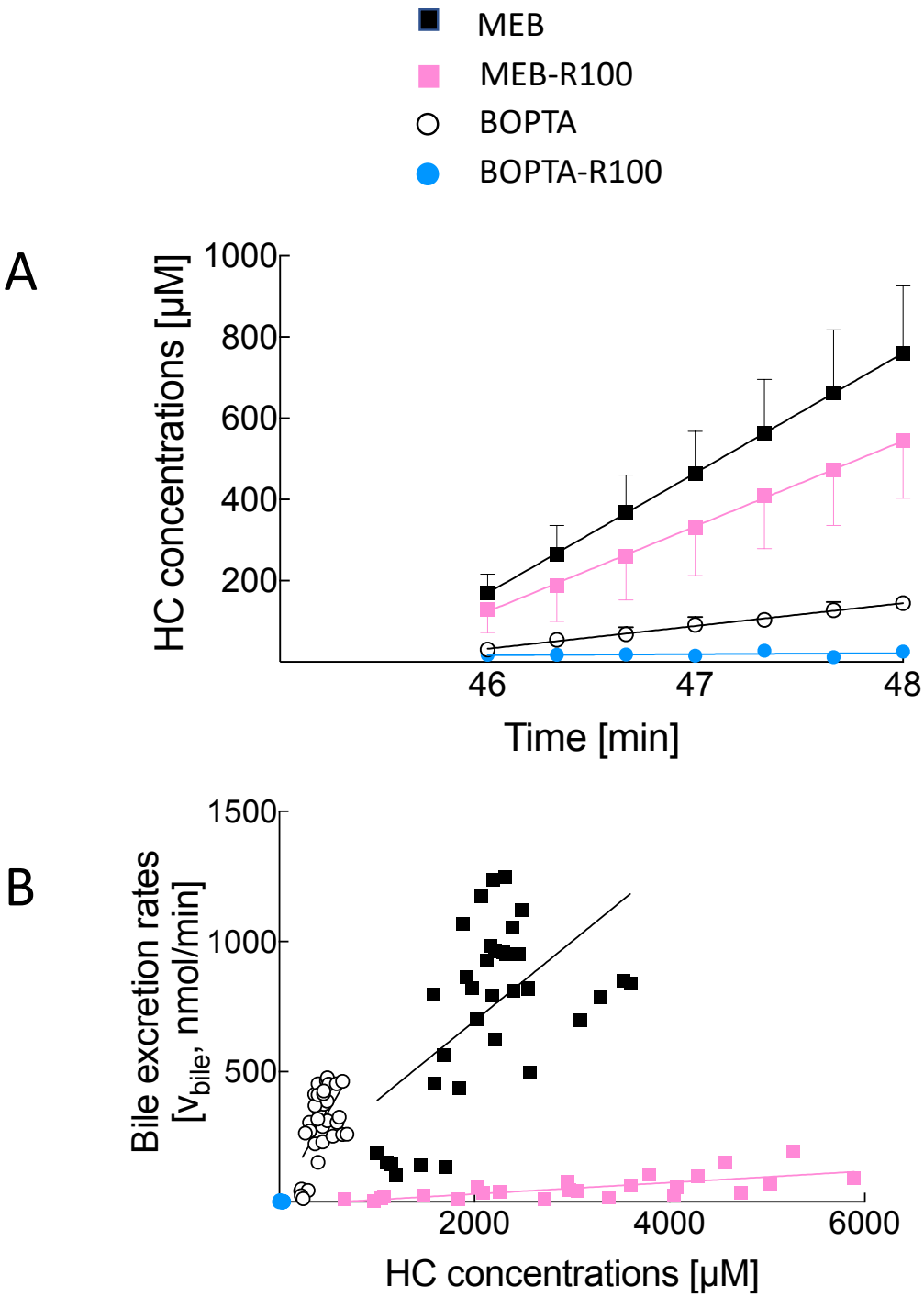
MEB
MEB-R100
BOPTA
BOPTA-R100
A
HC concentrations [µM]
1000
800
600
400
200
46
47
48
Time [min]
B
Bile excretion rates
[v_{bile}, nmol/min]
1500
1000
500
2000
4000
6000
HC concentrations [µM]